Environmental Science & Technology

Article

Cite This: Environ. Sci. Technol. 2018, 52, 10369−10379

pubs.acs.org/est

Formation and Physicochemical Characteristics of Nano Biochar: Insight into Chemical and Colloidal Stability

Guocheng Liu,[†] Hao Zheng,[‡] Zhixiang Jiang,[§] Jian Zhao,[‡] Zhenyu Wang,*[,†] Bo Pan,[∥] and Baoshan Xing*[,⊥]

[†]Institute of Environmental Processes and Pollution Control, and School of Environmental and Civil Engineering, Jiangnan University, Wuxi 214122, China

[‡]College of Environmental Science and Engineering, and Key Laboratory of Marine Environment and Ecology, Ministry of Education, Ocean University of China, Qingdao 266100, China

[§]College of Environmental Science and Engineering, Qingdao University, Qingdao 266071, China

[∥]Faculty of Environmental Science and Engineering, Kunming University of Science and Technology, Kunming 650500, China

[⊥]Stockbridge School of Agriculture, University of Massachusetts, Amherst, Massachusetts 01003, United States

Supporting Information

ABSTRACT: Nano biochar (N-BC) attracts increasing interest due to its unique environmental behavior. However, understanding of its formation, physicochemical characteristics, and stability of N-BC is limited. We therefore examined N-BC formation from bulk biochars (B-BCs) produced from peanut shell, cotton straw, Chinese medicine residues, and furfural residues at 300−600 °C. Carbon stability and colloidal processes of nano peanut shell biochars (N-PBCs) were further investigated. N-BCs formed from pore collapse and skeleton fracture during biomass charring, breakup due to grinding, and sonication. Amorphous fraction in B-BCs was more readily degraded into N-BCs than graphitic component. The sonication-formed N-PBCs contained 19.2−31.8% higher oxygen and fewer aromatic structures than the bulk ones, leading to lower carbon stability, but better dispersibility in water. Heteroaggregation of N-PBCs with goethite/hematite destabilized initially and then restabilized with increasing concentrations of N-PBCs. Compared with stacked complexes of N-PBCs-hematite, the association of goethite with N-PBCs could form interlaced heterostructures, thus shielding positive charges on goethite and causing greater heteroaggregation. These findings are useful for better understanding the formation of N-BCs and their environmental fate and behavior in soil and water.

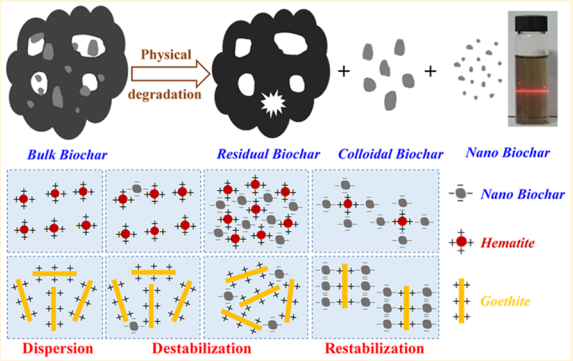

INTRODUCTION

Biochar (BC) produced from biomass pyrolysis has gained increasing attention from scientists, policymakers, farmers, and investors.[1−3] Generally, bulk BCs (B-BCs, 0.04−20 mm) are often employed for agronomic and environmental benefits.[4] Recently, several studies reported the physical degradation of B-BCs into nanoscale particles.[5,6] In comparison with B-BC, nano BC (N-BC) with size smaller than 100 nm was declared to have excellent mobility in natural soils and even transport into groundwater.[6,7] As a carrier, N-BC could facilitate the migration of natural solutes and contaminants, in contrast with positive effects of B-BC such as holding nutrients and immobilizing hazardous chemicals.[2,3] For instance, Chen et al. reported that BC nanoparticles (NPs) undesirably increased P leaching in alkaline soil.[8] Kim et al. also reported the enhancement of desorption and mobility of As in soil by BC fraction below 0.45 μm.[9] There are reports on the toxicity of carbonaceous nanomaterials such as carbon nanotubes (CNTs),[10] fullerene,[11] and graphene oxide (GO)[12] to plants, animals, and microorganisms. The toxic effect of NPs is generally considered to be higher than that of bulk particles.[13] Similar to engineered carbon nanomaterials, N-BC exposure may also trigger risks to organisms in waters and soils. Moreover, with increasing application of BCs into soils, more N-BCs will form and accumulate, thus making their environmental impact more significant. Therefore, the formation of N-BC and its potential fate in natural environments should be carefully examined and understood. However, current understanding on the formation pathways of N-BC is rather limited.

The physicochemical properties of B-BCs, depending on feedstock and pyrolytic temperature, have been extensively characterized.[14] However, limited studies pay attention to the characteristics of BC particulates with small size, especially N-

Received: March 20, 2018
Revised: July 25, 2018
Accepted: August 24, 2018
Published: August 24, 2018

DOI: 10.1021/acs.est.8b01481
Environ. Sci. Technol. 2018, 52, 10369−10379

BCs. Spokas et al. reported that hardwood BC fragments at microscale and nanoscale resulted from water erosion showed no detectable alteration on O/C atomic ratio relative to the B-BC (500 °C).[5] Conversely, others observed that BC fractions below 0.45 μm contained more polar groups and less aromatic clusters than the larger BCs (1−150 μm) from rice straw or bamboo produced at 400 °C.[15] Wang et al. also reported that wheat straw-derived N-BCs (350 °C and 550 °C) carried more negative charges than the micrometer-particles at pH 6.8.[6] The differences in the properties of these N-BCs may be associated with the original characteristics of their B-BCs. Thus, it is essential to systematically investigate the physicochemical characteristics of N-BCs. Braadbaart et al.[15] reported that physical fragmentation of B-BCs into small pieces was more pronounced for low-temperature BCs (≤400 °C). Keiluweit et al.[17] proposed the transition from scattered amorphous char (aliphatic and aromatic units incorporated with oxygen-containing groups) into ordered and dense tubostratic char (graphitic crystallites) as charring temperature increases. We therefore hypothesize that amorphous matrix in B-BCs may be more readily degraded into N-BCs than graphitic components. Moreover, the amorphous fraction with higher O content has been commonly considered to be more labile and easily decomposed,[18] thus, N-BCs likely exhibit lower carbon sequestration potential than B-BCs.

Aggregation between different colloids plays an important role in their environmental behaviors.[19] In water and soil environments, N-BCs will inevitably contact with natural minerals. Thus, heteroaggregation of N-BCs with mineral particles merits investigation. Deposition of clay-Ag/TiO_2 NPs[20] and hematite-SiO_2[21] after heteroaggregation was extensively reported. In contrast, no interaction occurred between graphene oxide (GO) and montmorillonite/kaolinite,[22,23] and GO even facilitated goethite dispersion.[23] These heteroaggregation behaviors between engineered NPs and minerals are primarily governed by electrostatic interaction. Indeed, electrostatic attraction-induced heteroaggregation could also be highly influenced by mass ratio of the two types of particles. For example, Feng et al. recently reported the heteroaggregation rate of GO-hematite first increased and then decreased with increasing GO concentrations.[24] For N-BCs, heteroaggregation with minerals (e.g., goethite and hematite) may also vary with N-BCs at different concentrations. As a result, N-BCs likely display different environmental fates in natural environments.

The main objectives of this study were therefore to (1) explore the pathways of N-BC formation, (2) characterize the differences between N-BCs and B-BCs, and (3) examine the chemical and colloidal stability of N-BCs. These findings can provide new insights toward understanding the degradation of B-BCs during the production and application, and the environmental behavior of N-BCs.

MATERIALS AND METHODS

Preparation of BC Samples. Peanut shell, cotton straw, Chinese medicine residues (mixture of *polygonatum sibiricum* and other herbs after pharmaceutical production), and furfural residues predried (80 °C) were respectively carbonized at 300−600 °C for 2 h under 500 mL/min N_2 flow in a tube furnace (O-KTF1200, Chunlei, China) into BC (PBC, CBC, MBC, and FBC).[25] B-BCs (75−150 μm) were sifted out from these BC samples, which are hereafter named as B-PBC*X*, B-CBC*X*, B-MBC*X*, and B-FBC*X*, respectively, where *X* is the pyrolytic temperature. All the B-BCs were rinsed with deionized water to remove excessive water-soluble minerals.

Extraction of N-BCs. A 0.7 g B-BC with 35 mL deionized water in a 40 mL vial was dispersed for 15 min at 25 °C under sonication at 120 W (FB120, Fisher Scientific, U.S.A.). Considering the neutral pH of most soils and their strong buffering capacity, the suspension pH was adjusted to 6.8 ± 0.1 by adding either 0.1 M HCl or NaOH solution. The suspension was set quiescently for 24 h to settle the particles larger than 1000 nm,[15] and the N-BC with size ≤100 nm was retained by centrifugation of the remaining suspension at 4200*g* for 30 min based on the Stokes' Law.[26] The settled and centrifuged BC fractions were defined as residual BC (R-BC, > 1000 nm) and colloidal BC (C-BC, 100−1000 nm), respectively. The above process was repeated five times, and the N-BC suspension was carefully pipetted and collected.

Hydrodynamic diameters (D_h) of C-BCs and N-BCs were measured by a Zetasizer (Nano ZS90, Malvern, U.K.). The extracted suspension (3 mL) was carefully moved to a quartz cuvette and examined at 800 nm (OD_{800}) using a UV−vis spectrophotometer (Lambda 35, PerkinElmer, U.S.A.).[23] Total C concentration of the suspension before and after filtrating through regenerated cellulose membrane (pore size, ∼3 nm) (Millipore, Germany) was determined by a TOC-VCSN (Shimadzu, Japan) for calculating the yield of N-BCs. The yield calculation of R-BCs, C-BCs, and N-BCs is presented in the Supporting Information (SI). All the treatments were conducted in triplicate at least.

Characterization of BC Samples. The pH, ash content, and surface area (SA) of R-BC, C-BC, and N-BC fractions extracted from B-PBCs (R-PBC*X*, C-PBC*X*, and N-PBC*X*, where *X* represents the charring temperature) were characterized.[27] Total C, H, N, and O content were measured with an elemental analyzer (MicroCube, Elementar, Germany). Scanning electron microscopy (SEM, S4800, Hitachi, Japan), transmission electron microscopy (TEM, H-7650, Hitachi, Japan), and atomic force microscopy (AFM, 5400, Agilent, U.S.A.) were employed to observe the morphology of N-PBCs. The samples were further characterized using Fourier transform infrared spectroscopy (FTIR, Tensor 27, Bruker Optics, Germany), X-ray photoelectron spectroscopy (XPS, ESCALAB 250Xi, Thermo scientific, U.S.A.), Raman spectroscopy (DXR Raman Microscope, Thermo Scientific, U.S.A.), and X-ray diffraction (XRD, D8 Advance, Bruker, Germany). The details of these characterization methods are provided in the SI.

Measurement of BC Carbon Stability. The carbon chemical stability of B-PBCs, R-PBCs, C-PBCs, and N-PBCs was evaluated by oxidation with hydrogen peroxide (H_2O_2).[28] Briefly, 0.1 g of BC was added into a 40 mL glass vial with 7 mL of 5% H_2O_2, and treated at 80 °C for 48 h. Subsequently, the C content in BC before and after H_2O_2 oxidation was measured by the elemental analyzer, and their mass was weighed. As an indicator of BC stability, residual C percentage was calculated on the basis of the mass and C content. In addition, mass loss of BC varying with temperature was performed by a thermogravimetric analyzer (TGA, STA-449-F3, Netzsch-Geratebau GmbH, Selb, Germany) at a rate of 10 °C/min from 30 °C to 700 °C under air atmosphere at 100 mL/min.

Aggregation Kinetic of N-PBC in Aqueous Phase. The aggregation of N-PBCs was investigated using NaCl as destabilization electrolyte.[24] The N-PBC suspension was sonicated for 5 min to achieve stability and diluted to a

DOI: 10.1021/acs.est.8b01481
Environ. Sci. Technol. 2018, 52, 10369−10379

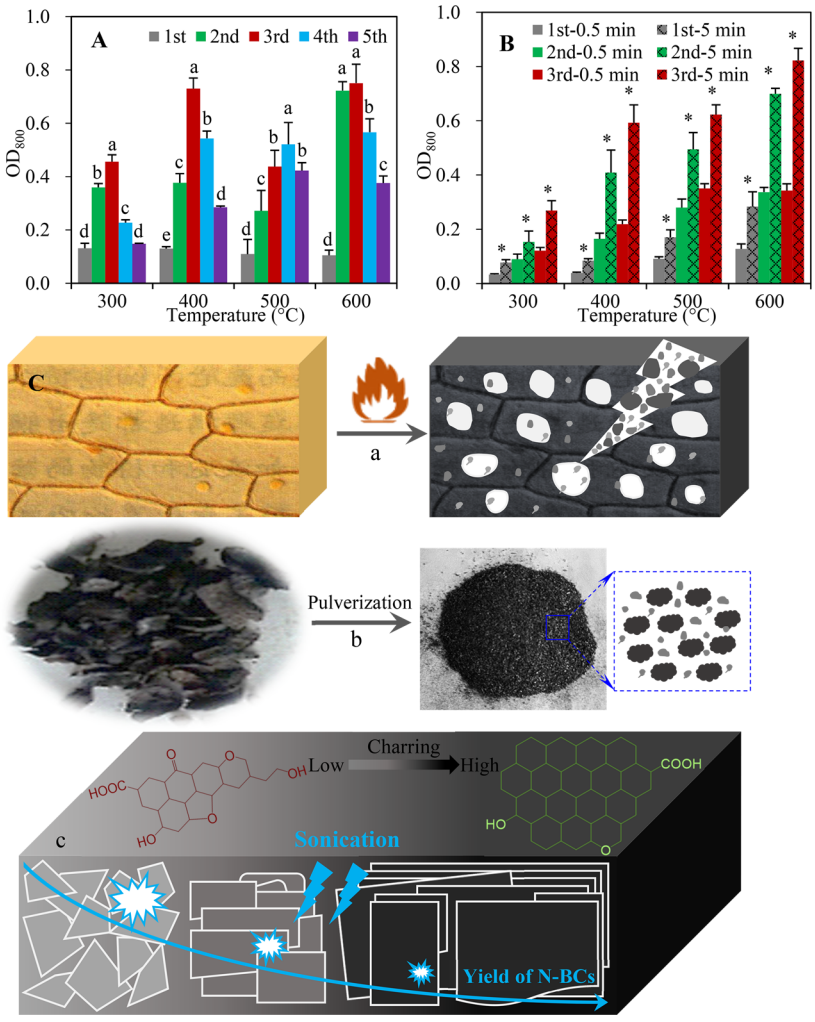

Figure 1. Release of nano biochar (N-BC) from (A) peanut shell-derived biochars (PBCs, 75−150 μm) during the five consecutive extraction processes and (B) the pulverized PBCs for 0.5 and 5 min, respectively. (C) Possible pathways of N-BC formation from B-BC: (a) pore collapse and carbon matrix fracturing during pyrolysis, breakup due to grinding, and (c) sonication. For a given temperature, the different letters indicate significant difference among the N-BC release in the five consecutive extraction processes, and the asterisk represents significant difference between the N-BC release from PBCs ground for 0.5 and 5 min (n = 3, p < 0.05).

desired concentration (100 mg C/L). One milliliter of the suspension was mixed with 1 mL NaCl solution (0−800 mM) in a cuvette, and immediately analyzed by dynamic light scattering (DLS) (100 measurements, 15 s autocorrelation accumulation time, 5 s delay between measurements) using the ZS90 for monitoring the D_h values. Critical coagulation concentration in NaCl solution (CCC_{NaCl}) of N-PBCs was calculated by normalizing initial growth rate of D_h.[24]

Heteroaggregation of N-PBC with Natural Mineral Particles. Goethite (Goe) was treated by ultrasonic dispersion and centrifugation.[29] Briefly, the slurry of Goe (Sigma-Aldrich) fines in deionized water was sonicated for 30 min and centrifuged at 1900g for 24 min to obtain its colloidal suspension. Then the suspension was freeze-dried into Goe powders. Hematite NPs (Hem) was purchased from Aladdin Reagent Co. (China). The Na-saturated minerals were obtained via cation exchange in 0.5 M NaCl and washing with deionized water.[23] These Na-saturated minerals were employed to avoid possible influence of mixed exchangeable cations (e.g., Na^+, K^+, and Ca^{2+}) on the interaction of minerals with N-PBCs. The suspensions of minerals (20 mg/L) were prepared by suspending the two minerals in deionized water under sonication at 120 W for 5 min, respectively. Goe or Hem suspension was injected with the same volume of N-PBC300 or N-PBC600 suspension in a cuvette, and then measured immediately by DLS after shaking. Under the conditions of present work, the scattered-light intensity of minerals is much greater than that of N-PBCs during the DLS measurement. That is, the measured D_h in the binary systems mainly represents that of free minerals and the minerals incorporated in heteroaggregates. Thus, the heteroaggregation of minerals with N-PBCs can be studied by this technique.[24]

RESULTS AND DISCUSSION

N-BC Formation. The extraction from B-PBC300 and B-PBC600 turned from brown to much lighter-colored or even colorless after filtration through regenerated cellulose membrane (pore size, ~3 nm) (Figure S1A, B), indicating that the extracted suspensions contained fine PBC particles. The tyndall effect, an effect of light scattering in colloidal dispersion, was used to further confirm the existence of PBC particulates in the suspensions (Figure S1C). Their D_h values were ~180−350 nm (Figure S2A), close to that of GO (~267 nm)[30] and CNTs (160 nm).[31] The OD_{800} values of these

DOI: 10.1021/acs.est.8b01481
Environ. Sci. Technol. 2018, 52, 10369−10379

Table 1. Yield and Physicochemical Properties of the Different Fractions of Biochar

	yield[b] %		elemental content %				atomic ratio						
samples[a]	0.7 g:35 mL	8.0 g:400 mL	C	H	O	N	H/C	O/C	(O+N)/C	pH	ash %	SA[c] m^2/g	ID/IG[d]
B-PBC300	100	100	55.4	3.97	21.0	1.97	0.86	0.28	0.31	6.61 ± 0.04b[e]	13.1 ± 0.1a	3.67	0.95 ± 0.01a
R-PBC300	77.8 ± 2.9	76.0 ± 6.2	66.8	3.97	23.2	0.97	0.71	0.26	0.27	6.89 ± 0.02a	8.19 ± 0.36b	7.23	0.83 ± 0.00c
C-PBC300	12.4 ± 1.1	14.4 ± 2.1	50.9	3.57	22.3	1.31	0.84	0.33	0.35	6.51 ± 0.09bc	5.42 ± 0.61d	19.0	0.89 ± 0.01b
N-PBC300	2.36 ± 0.08	1.41 ± 0.11	50.2	3.67	26.6	1.94	0.88	0.40	0.43	6.40 ± 0.04c	6.89 ± 1.14c	63.6	0.87 ± 0.01b
B-PBC400	100	100	60.1	3.56	17.2	1.92	0.71	0.21	0.24	7.59 ± 0.05a	13.4 ± 0.1a	4.75	0.86 ± 0.00a
R-PBC400	78.1 ± 5.1	76.5 ± 1.8	70.2	3.60	18.9	0.95	0.62	0.20	0.21	7.04 ± 0.04b	8.74 ± 0.81b	9.37	0.76 ± 0.04b
C-PBC400	12.6 ± 1.6	13.5 ± 1.0	57.9	3.80	17.4	2.20	0.79	0.23	0.26	6.87 ± 0.06c	8.87 ± 1.53b	19.4	0.81 ± 0.02ab
N-PBC400	1.95 ± 0.10	1.06 ± 0.09	54.8	3.68	20.5	2.15	0.81	0.28	0.31	6.80 ± 0.03c	7.68 ± 0.46b	78.6	0.81 ± 0.01ab
B-PBC500	100	100	61.3	2.69	12.0	1.66	0.53	0.15	0.17	8.48 ± 0.05a	14.3 ± 0.1a	7.34	0.85 ± 0.05a
R-PBC500	83.4 ± 6.0	83.6 ± 2.1	78.0	2.91	10.7	0.91	0.45	0.10	0.11	7.57 ± 0.03b	8.64 ± 0.64c	11.5	0.77 ± 0.00b
C-PBC500	9.59 ± 1.42	8.56 ± 0.50	60.3	2.99	13.1	1.69	0.60	0.16	0.19	7.15 ± 0.02c	11.2 ± 1.2b	49.6	0.82 ± 0.01ab
N-PBC500	1.05 ± 0.12	0.54 ± 0.07	61.1	3.55	15.7	2.22	0.70	0.19	0.22	7.08 ± 0.04c	8.93 ± 0.34c	230	0.82 ± 0.04ab
B-PBC600	100	100	64.3	2.04	9.16	1.40	0.38	0.11	0.13	9.81 ± 0.04a	16.5 ± 0.3a	8.82	0.85 ± 0.02a
R-PBC600	86.5 ± 3.6	86.9 ± 2.4	82.2	2.16	6.72	0.79	0.32	0.06	0.07	7.90 ± 0.08b	9.29 ± 0.88c	13.8	0.74 ± 0.03b
C-PBC600	8.46 ± 0.71	6.89 ± 0.87	64.9	2.07	9.50	1.45	0.38	0.11	0.13	7.29 ± 0.05c	14.3 ± 0.4b	48.8	0.82 ± 0.02a
N-PBC600	0.87 ± 0.05	0.47 ± 0.04	61.4	1.92	11.9	1.11	0.38	0.15	0.16	7.27 ± 0.03c	9.16 ± 0.94c	264	0.83 ± 0.01a

[a]B-PBC*X*, R-PBC*X*, C-PBC*X*, and N-PBC*X* are the bulk, residual, colloidal, and nano biochars from peanut shell, respectively, where *X* represents pyrolytic temperature. [b]Yield of different fractions of PBC was calculated from the extraction for N-PBC suspension from 0.7 g B-PBC in 35 mL deionized water and the preparation of N-PBC powders from 8.0 g B-PBC in 400 mL deionized water, respectively. [c]SA is the surface area calculated by Brunauer−Emmett−Teller model. [d]ID/IG is the intensity ratio of D band to G band of the biochars by Raman spectroscopy. [e]The different letters behind the data represent significant difference among the biochar fractions ($n = 3$, $p < 0.05$).

Environ. Sci. Technol. 2018, 52, 10369−10379
DOI: 10.1021/acs.est.8b01481

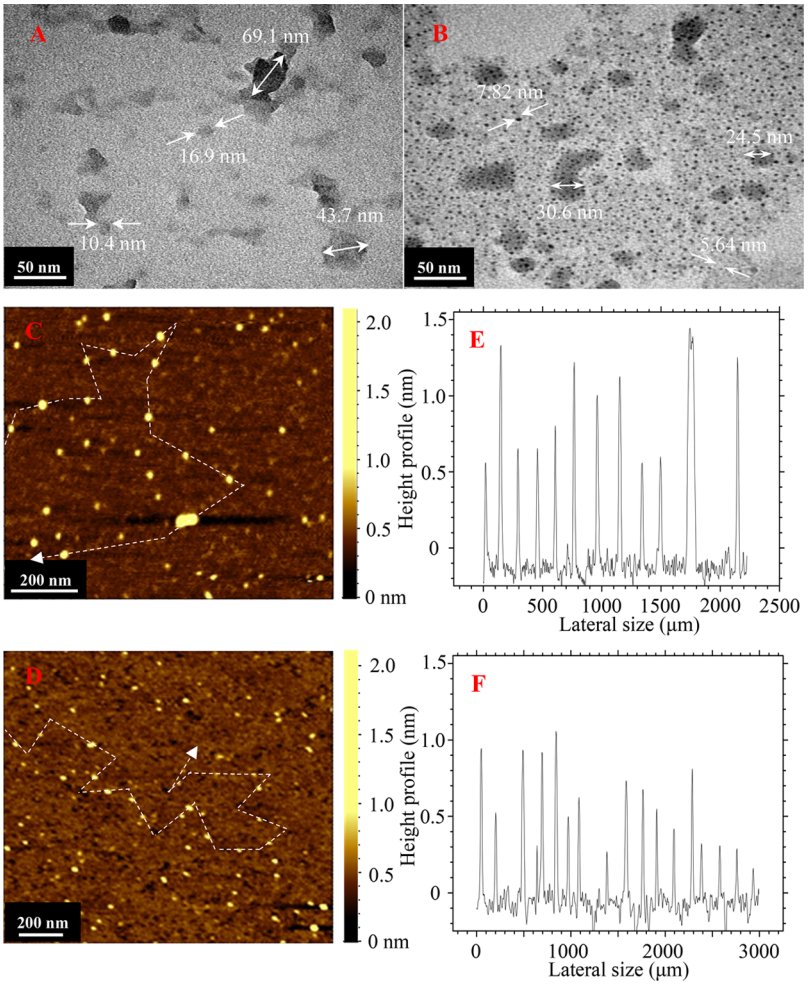

Figure 2. TEM images of (A) N-PBC300 and (B) N-PBC600. AFM images of (C) N-PBC300 and (D) N-PBC600. The diameter (lateral size, *x*-axis) and thickness (height profile, *y*-axis) analysis of (E) N-PBC300 and (F) N-PBC600 particles on the dotted line in panel (C) and (D).

suspensions ranged from 0.11 to 0.75 during the five consecutive extraction processes (Figure 1A), significantly greater than those of their ultrafiltrates (<0.002). Thus, the OD_{800} values were primarily resulted from the dispersion of N-PBCs, and the contribution from DOC could be ignored. These results demonstrated the release of N-PBCs from B-PBCs. Similarly, N-BC release from B-CBCs, B-MBCs, and B-FBCs also occurred (Figures S2B–D and S3–5).

SEM images showed fine fragments scattered on the surface and inner pores of untreated B-PBCs (Figure S6A, B), and obvious crevices were observed in the carbon matrix of B-PBC600 (Figure S6B). Much is known about pore collapse of BCs at relatively high temperatures (≥500 °C).[32] Presumably, N-BC is generated from the destruction of pores and carbon matrix during BC production. The higher OD_{800} values of the suspensions extracted from heavily ground PBCs (5 min) than those from slightly ground PBCs (0.5 min) indicated the formation of higher amount of N-PBCs with longer grinding time (Figure 1B). Previous work by Manikandan et al.[33] also reported that the size of B-BC (<0.5 mm) reduced to nanoscale level (D_h, 260 nm) after 6 h ball milling. The negligible turbidity of the supernatants without Tyndall effect suggested that little N-PBCs released from all the B-PBCs in the nonsonication treatment (Figure S4). However, N-PBCs were dramatically released after sonication (Figure S5). The fine fragments adhered to the surface or were embedded in the pores of B-PBCs were exfoliated by sonication (Figure S6A–D), leading to N-PBC release. Interestingly, numerous sites of the carbon matrix in R-PBC300 were eroded, while the erosion was not observed in R-PBC600 (Figure S6C–F), suggesting that B-PBC300 appeared to degrade more easily than B-PBC600. More N-PBCs were extracted from smaller B-PBCs (75–150 μm) than larger ones (0.85–2 mm) due to more surface exposure of fragile matrixes (Figure S7). Additionally, N-PBC release initially increased and then decreased following the repeated extraction (Figure 1A), indicating that longer sonication likely triggered more N-PBC formation, whereas R-PBCs became more stable and difficult to physically disintegrate. This may be related to heterogeneous carbon categories in B-PBCs (e.g., aliphatic, aromatic, and graphitic components), which is discussed later.

Overall, three pathways of N-BC formation were identified: (a) pore collapse and matrix fracture during biomass charring, (b) breakup due to grinding, and (c) sonication (Figure 1C). If particle size has to be reduced (e.g., BC produced from large wood pieces), mild grinding is commonly used for minimizing physical disintegration, which is also a good management practice to avoid wind loss.[34] The latter two processes are commonly used to mimic physical weathering of charcoal and minerals.[5,29,35] Natural weathering such as drying–wetting and freeze–thaw cycles could cause physical stress (e.g., abrasion and swelling) on fossil charcoal and geologic minerals. For BC

DOI: 10.1021/acs.est.8b01481
Environ. Sci. Technol. 2018, 52, 10369–10379

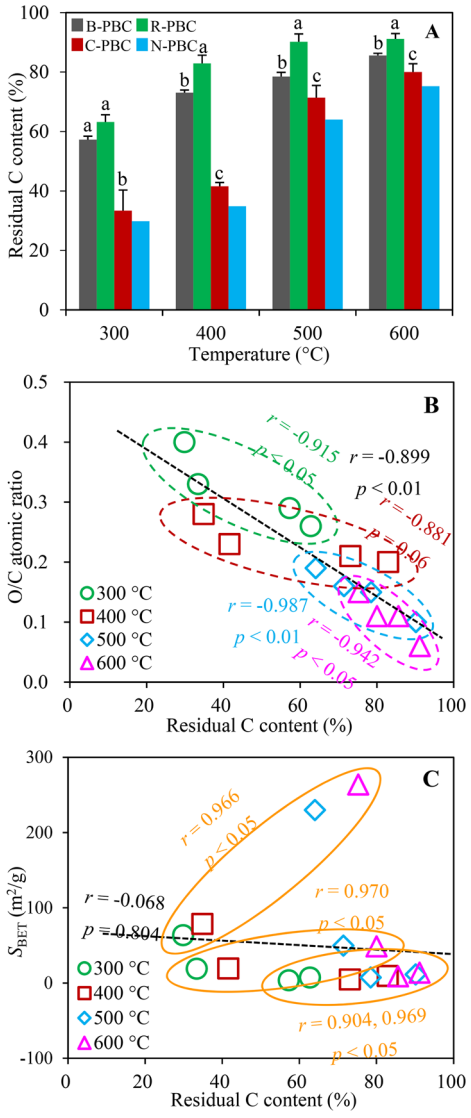

Figure 3. Chemical stability of different biochars. (A) Residual C content of the different fractions of peanut shell-derived biochars (PBCs) after H_2O_2 oxidation for 48 h. (B) Correlations between the residual C content and O/C atomic ratio for different biochar fractions. (C) Correlations between the residual C content and surface area (S_{BET}) for different biochar fractions. In panel (A), different letters indicate significant difference among the biochar fractions ($n = 3$, $p < 0.05$). In panels (B and C), black dashed lines represent the correlations based on the data of all the biochar samples; for a given temperature, the correlations are presented by different color dashed ellipses; and for a biochar fraction, yellow solid ellipses indicate the correlations between the residual C content and pyrolytic temperature. The correlation coefficients (r and p value) were obtained from Pearson correlation analysis.

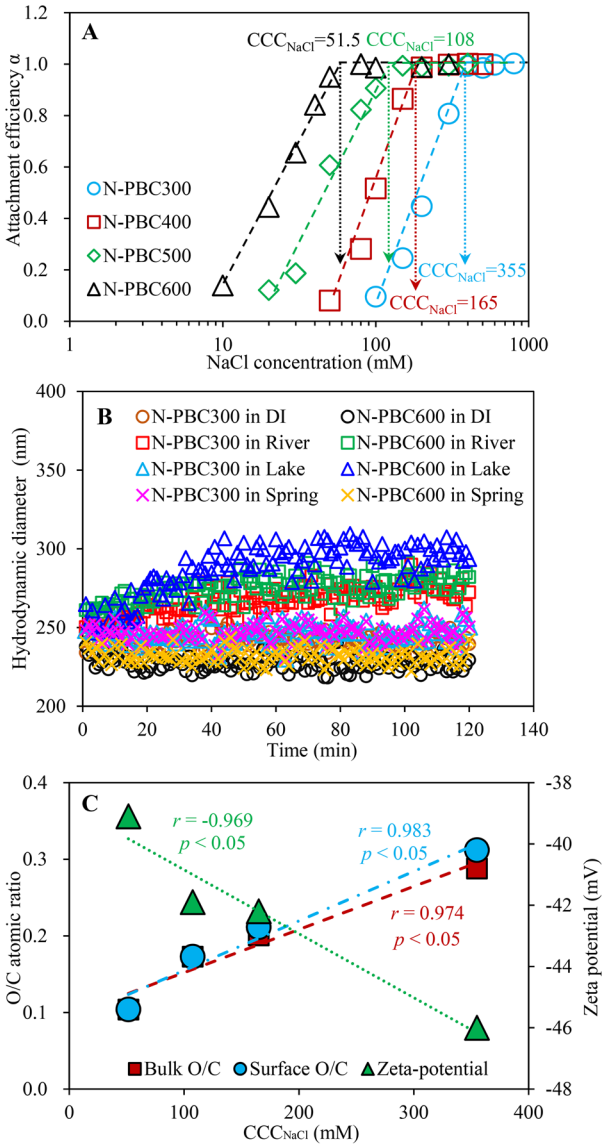

Figure 4. Dispersibility of N-PBCs in water. (A) Aggregation attachment efficiencies of N-PBCs in the presence of NaCl at pH 6.8. (B) Aggregation kinetics of N-PBC300 and N-PBC600 in natural waters. (C) Correlations between critical coagulation concentrations of NaCl (CCC_{NaCl}) of N-PBCs and their bulk and surface O/C atomic ratios, or zeta potentials at pH 6.8, respectively. The natural waters from Licun river, Jihongtan lake, and Laoshan spring in Qingdao (China) were employed in this study.

particles, this weathering process could also occur in natural environments, thus leading to their physical disintegration into smaller fragments such as N-BC. Therefore, processes (b) and (c) are the effective approaches to simulate physical weathering of BC in natural conditions,[5,15,36] and the physiochemical properties of the obtained N-BCs could be close to those of N-BCs formed under natural conditions. It should be noted that abiotic and microbial aging can mineralize unstable organic components in BC.[37] In the BC−root interface, fine roots and root hairs stress the physical structure of BC through extending or exploring across BC surface and pores;[38] root-derived organic acids may erode BC matrix.[39] The role of biological reactions in the fragmentation of BC needs further investigation.

Yield of N-BCs. The yield of N-PBCs from B-PBCs followed an order: N-PBC300 (1.41−2.36%) > N-PBC400 (1.06−1.95%) > N-PBC500 (0.54−1.05%) > N-PBC600 (0.47−0.87%), opposite that of R-PBCs (Table 1), implying that N-BC formation may be closely associated with the temperature-dependent heterogeneities of B-BCs. With increasing temperature, graphitic crystallites in BC incrementally grew at the expense of amorphous components (e.g., aliphatics and small (poly)aromatic units),[40] and the graphitic crystallites are ordered, denser, and rigid relative to the amorphous phase.[16,17] Thus, we speculate that the less carbonized fractions

DOI: 10.1021/acs.est.8b01481
Environ. Sci. Technol. 2018, 52, 10369−10379

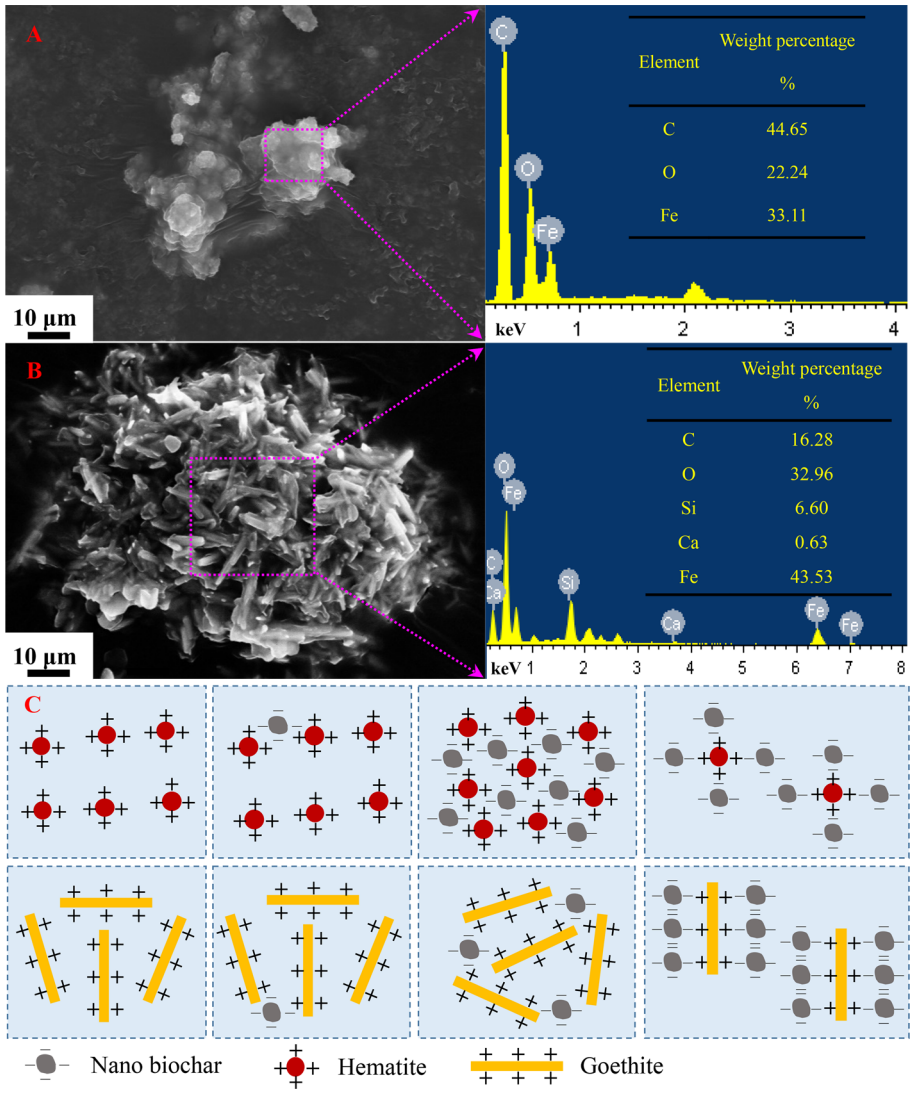

Figure 5. SEM images of (A) Hem+N-PBC600 and (B) Goe+N-PBC600 at the peak heteroaggregation concentration. EDX spectra of the heteroaggregates were collected from pink frames. (C) Possible configurations of the heteroaggregates of Hem or Goe and N-PBC at different N-PBC concentrations.

in B-BCs are prone to be physically disintegrated into N-BCs, as illustrated in Figure 1c. To test this hypothesis, activated carbons from coal and coconut husk and natural graphite with different carbon categories were selected to examine the release of NPs. Expectedly, few NPs were released from graphite and coal activated carbon, but the NP release was clearly observed from coconut husk activated carbon that contains abundant amorphous units (Figure S7). It is noted that the yields of C-PBCs were much higher than those of N-PBCs (6.89−14.4% vs 0.47−2.36%, Table 1). Consequently, special attention is warranted on the environmental behavior (e.g., transport, transformation, and biological effects) of C-PBCs under natural conditions.

The release of nano FBCs (N-FBCs) from B-FBCs was negligible in initial three extraction treatments (OD_{800} < 0.03, Figures S3A and S5B). The N-FBC release occurred at the fourth extraction, but their OD_{800} values were significantly lower than those from B-PBCs, B-CBCs, and B-MBCs (Figures 1A and S3), thus lower level of N-FBC formation. It was ascribed to more graphitic structures in B-FBCs from carbonizing higher content of lignin (45.2% vs 12.1−23.4%) and less cellulose (22.1% vs 38.9−48.2%) in FR compared with those in other feedstocks (Figure S8A).[17,41] This was well supported by much lower O/C ratios of B-FBCs than B-PBCs, B-CBCs, and B-MBCs in Van Krevelen diagram (Figure S8B) and lower intensity ratios of D to G band (ID/IG) in Raman analyses (Tables 1 and S1). The lower formation of N-FBCs further confirmed higher friability of carbon fraction with lower degree of carbonization. Oppositely, Spokas et al.[5] reported that wood-derived B-BC was readily broken into N-BC than those produced from grass and corn stalk with higher-cellulose content after being rinsed with water for 24 h. The differences in N-BC formation are possibly associated with physical parameters (e.g., hardness and abrasion resistance) of B-BCs, mostly depending on morph-physiological diversity of feedstock and pyrolysis condition (mainly temperature), which deserves further investigation. N-PBC, N-CBC, and N-MBC were much easier to be formed than N-FBC as indicated by OD_{800} values. To simplify the following experimental systems, N-PBC was selected as a representative N-BC for the characterization, carbon stability, and heteroaggregation investigations.

DOI: 10.1021/acs.est.8b01481
Environ. Sci. Technol. 2018, 52, 10369−10379

Characterization of N-PBCs. TEM images showed that N-PBC300 and N-PBC600 were nanoscale solids (Figure 2A, B). AFM observation further confirmed the nanoscale size of N-PBC300 ((17.4 ± 4.2) nm) and N-PBC600 ((25.3 ± 11.9) nm) (Figure 2C−F). The diameter of N-PBC300 and N-PBC600 was comparable with (or even smaller than) commercial nano graphite ((56.4 ± 15.1) nm, Figure S9) and pecan shell N-BC (30−500 nm) reported by Yi et al.[19] Notably, the thickness (height profile) of N-PBC300 and N-PBC600 was in the range of 0.69−1.61 nm and 0.36−1.22 nm, respectively, which is very close to that of GO (0.5−1.2 nm).[22,42,43] C-PBC300 and C-PBC600 had flake-like morphology with the lateral size at ∼0.46−2.6 and ∼0.23−2.1 μm, respectively. Some of C-PBCs were smooth and globular features (red arrows, Figure S10A−D), but others showed angular and sharp-edged shapes (blue arrows, Figure S10A−D). Moreover, the thickness of C-PBC300 and C-PBC600 was at nanometer level (<4 nm, Figure S10E−H).

Both total and surface C contents of R-PBCs were markedly higher than those of B-PBCs, and N-PBCs contained the highest O and lowest C contents (Tables 1 and S2). The O/C ratios of N-PBCs were much higher than those of R-PBCs, indicating more O-containing functional groups (OFGs) on N-PBCs. This was supported by stronger peaks of C−O−C stretching or aliphatic −OH (1030 cm^{-1}), phenolic −OH (∼1375 cm^{-1}), and C−O (∼1261 cm^{-1}) in N-PBCs (Figure S11).[15,17] Consistently, N-PBCs contained more surface OFGs, including phenolic or ether C−O, ketone C═O, and carboxylic COO, than R-PBCs (Figure S12, Table S3). The relative contents of aromatic C (C−C/C═C/C−H) in N-PBC300 ((41.6 ± 0.27)%) and N-PBC600 ((73.4 ± 0.43)%) were significantly lower than those in R-PBC300 ((55.8 ± 0.17)%) and R-PBC600 ((81.1 ± 0.33)%) (Table S3). B-PBCs, similar to natural graphite, exhibited a sharp symmetric peak of graphite crystallite at ∼26.5° in their XRD spectra (Figures S13 and S14). In comparison with B-PBCs, undifferentiated graphite peak was observed in R-PBCs, whereas the intensity and pattern of graphite peak, closely related with abundance and size of graphitic C, were weakened and broadened in N-PBCs. Also, the greater ID/IG ratios of N-PBCs than R-PBCs implied more amorphous phase and fewer graphitic crystallites in N-PBCs using the Raman analyses (Table 1 and Figure S15). Our results were supported by the data from Qu et al.[15] that BC colloids possessed more OFGs and fewer aromatics than B-BC. Furthermore, the ash content in R-PBCs was lower than B-PBCs (Table 1), suggesting the minerals were separated from B-PBCs and/or dissolved during the N-PBC extraction. Compared with B-PBCs, N-PBCs had lower pH values due to more acidic OFGs (e.g., −COOH) and lower ash content. The dominant minerals in N-PBCs were SiO_2, CaC_2O_4, and $CaCO_3$ (Figure S13). These PBC fractions with heterogeneous properties probably display different carbon stability and colloidal behavior, which are discussed below.

Carbon Stability of N-PBCs. The chemical oxidation by H_2O_2 is usually employed to evaluate antioxidative capacity of BCs, reflecting long-term stability in natural environments.[28] The C loss with H_2O_2 oxidation followed the order: N-PBC > C-PBC > B-PBC > R-PBC (Figure 3A). The C loss percentage of N-PBC300 was 70.2%, for instance, 1.91, 1.81, and 1.05 times of those of R-PBC300, B-PBC300, and C-PBC300, respectively. The lower chemical stability of N-PBCs could be ascribed to their richer OFGs, and the highest aromatic fraction in R-PBCs were responsible for their greatest stability (Figures S11 and S15). These were supported by the negative relationship between the residual C content in the PBC fractions and their O/C or H/C ratios (Figures 3B and S17). In contrast with aromatic C, the C bonded with O (e.g., C−O−C and C═O) is more easily pyrolyzed in TGA measurement.[44] Thus, the highest mass loss of N-PBCs as a function of temperature (30−550 °C) relative to other fractions further suggested their lowest carbon stability (Figure S16). Taking the yields of N-PBCs and C-PBCs into consideration, their C loss in the H_2O_2 oxidation accounted for 0.81−4.72% and 9.54−29.3% of total C loss of B-PBCs, respectively, implying that the disintegration of B-PBCs to C-PBCs largely weakened the C sequestration potential in soils compared to N-PBCs. N-PBCs with strikingly greater SA (Table 1) may expose more active carbon sites than other fractions, leading to higher C loss.[28] However, for different PBC fractions, poor correlations were observed between residual C contents and SA (Figure 3C), implying that higher SA of N-PBCs was not the dominant factor for their lower chemical stability. Notably, for the same fraction, there were positive correlations between the residual C content and pyrolytic temperature (Figure 3C), suggesting that the carbon stability of PBCs was primarily controlled by the temperature-dependent chemical properties.

Dispersibility of N-PBCs in Aqueous Phase. D_h values of N-PBC suspensions increased with increasing concentrations of NaCl (Figure S18). Carbon fraction is the dominant ingredient ((90.84−93.11)%) of N-PBCs (Table 1). Thus, this D_h growth was primarily caused by the homoaggregation of C-containing particles rather than mineral particles in N-PBCs. The CCC_{NaCl} values of N-PBC300, N-PBC400, N-PBC500, and N-PBC600 were 355, 165, 105, and 51.5 mM (Figure 4A), respectively, close to or even higher than the reported CCC_{NaCl} values for CNTs (25 mM),[45] fullerene (120 mM),[46] GO (200 mM),[47] and pecan shell N-BC (250 mM).[19] The dispersion of N-PBCs in natural surface waters was further examined in the present work. Initially, the D_h of N-PBC300 and N-PBC600 increased slightly in river and lake waters (Figure 4B), perhaps because of cations (e.g., Na^+, Ca^{2+}, and Mg^{2+}) (Table S4), but after 1 h or even 5 days, these values still remained stable (∼300 nm, Figure S19). These results indicated high dispersibility of N-PBCs in aquatic environments. Electrostatic repulsion is the major force for a stable colloid system.[48] The lower-temperature N-PBC had more negative charges (Figure S20) mainly resulting from the ionization of more −COOH groups at pH 6.8 (Table S3), thus showing better colloidal stability. This was well supported by the significant and negative correlation between the CCC_{NaCl} values and the zeta potentials (Figure 4C). The positive correlation of the CCC_{NaCl} values with the surface O/C ratios (Figure 4C) further confirmed the temperature-dependent dispersibility of N-PBCs.

Heteroaggregation of N-PBCs with Natural Minerals. The heteroaggregation of N-PBCs with Goe/Hem depended strongly on the concentrations of N-PBC300 and N-PBC600 (Figure S21). For example, D_h and D_h growth rate of Goe increased with increasing N-PBC300 concentrations from 0.05 to 0.5 mg C/L, while beginning to decline when N-PBC300 concentrations were above 0.5 mg C/L. For N-PBC300 concentrations higher than 25 mg C/L, Goe once again became stable. Smith et al. observed a similar destabilization−restabilization trend in the binary system of Hem and Au NPs

DOI: 10.1021/acs.est.8b01481
Environ. Sci. Technol. 2018, 52, 10369−10379

as a function of Au NP concentrations.[49] Further, in the present work, large solid complexes of Goe/Hem with N-PBC300/N-PBC600 were clearly observed (Figures 5A, B and S22), which can explain the sedimentation of Goe/Hem (100 mg/L) with N-BC (25 mg C/L) as reported in our previous study.[50]

For N-PBC600, the concentrations for the peak of D_h growth rate of Goe and Hem (heteroaggregation peak concentration) were 2.5 and 12.5 mg C/L, respectively, 4 and 3.2 times higher than that of N-PBC300 (Figure S22). Lower surface OFG content as indicated by XPS data (Table S3) and less negative charges on N-PBC600 than N-PBC300 (Figure S20) can explain the higher heteroaggregation peak concentration of N-PBC600. The heteroaggregation peak of Hem with N-PBC300 and N-PBC600 occurred at 3.0 and 12.5 mg C/L (Figure S22), respectively, much higher than the heteroaggregation peak concentrations of Goe+N-PBC300 and Goe+N-PBC600 (0.5 and 2.5 mg C/L). This is due to the difference in geometric dimension and shape of Hem and Goe. Thus, SEM was employed to investigate the configuration of Hem+N-PBCs and Goe+N-PBCs. After heteroaggregation, the stacked complexes of Hem+N-PBC300 and Hem+N-PBC600 were observed (Figures 5A and S22A), suggesting that Hem, as nanosphere with D_h of ∼128 nm, is likely to aggregate with N-PBCs through bridging. Dissimilarly, rod-shaped Goe particles (D_h, ∼473 nm) formed interlaced heteroaggregates with N-PBCs (Figures 5B and S22B), thus shielding a large proportion of positively charged sites on Goe and causing stronger heteroaggregation than Hem+N-PBCs. This "charge shielding" mechanism was proposed schematically in Figure 5C. Similarly, Sarpong et al. also found a crossed-network heteroaggregates between curled CNTs and spherical ZnS NPs.[51] The above heteroaggregation results confirmed that the association of two types of oppositely charged particles was largely influenced by the geometric characteristics of particles and specific particle−particle configuration.

■ ENVIRONMENTAL IMPLICATIONS

This study demonstrated that N-BCs could be generated from pore collapse and matrix fracturing during BC production and weathering process in the environment, and the fewer carbonized B-BCs were more easily degraded into N-BCs. N-BC formation may be susceptible to attachment of soil components onto B-BCs, such as pore blocking and particle wrapping by microorganism colonization and fine minerals adhesion.[52,53] The carbon matrixes that can be easily fragmentized are readily mineralized via chemical and microbial oxidation,[54] thus the priority or synergy among physical, chemical, and microbial aging on B-BCs deserves further investigation in field-incubation experiments. From our observations, the degradation of B-BCs into C-BCs and N-BCs was counted against BC longevity within soil systems. Higher pyrolytic temperatures (>500 °C) favor the C sequestration potential of BCs not only because of more stable structural properties,[18] but also due to their lower friability in soils. Also, we observed the interaction of N-BCs with natural minerals (e.g., Goe and Hem) into stable complexes, which are well-known to protect organic carbon against being mineralized.[55] Furthermore, vertical transport of N-BCs in soil profile may be retarded by heteroaggregation, thus the N-BCs-facilitated migration of soil contaminants is probably weaker than predicted.[6] However, given high dispersion of N-BCs in natural waters, they and associated contaminants may trigger exposure risk to aquatic organisms, similar to engineered carbonaceous nanomaterials.[56,57] The information presented here will be helpful for better understanding the aging processes of BCs and the fate and transport of N-BCs in natural environments.

■ ASSOCIATED CONTENT

Supporting Information

The Supporting Information is available free of charge on the ACS Publications website at DOI: 10.1021/acs.est.8b01481.

Correction of OD800 and yield of nano biochars; characterization of biochars; 22 figures, 4 tables, and additional references (PDF)

■ AUTHOR INFORMATION

Corresponding Authors

*Phone: +1 413 545 5212. E-mail: bx@umass.edu. (B.X.).
*Phone: +86 510 85911123. E-mail: wang0628@jiangnan.edu.cn (Z.W.).

ORCID

Jian Zhao: 0000-0002-4971-5643
Zhenyu Wang: 0000-0002-5114-435X
Bo Pan: 0000-0003-3680-1451
Baoshan Xing: 0000-0003-2028-1295

Notes

The authors declare no competing financial interest.

■ ACKNOWLEDGMENTS

This research was supported by Key Program of Natural Science Foundation of China (41530642), Natural Science Foundation of China (41503093, 41820104009, and 41573092), AoShan Talents Program Supported by Qingdao National Laboratory for Marine Science and Technology (No. 2015ASTP), Taishan Scholars Program of Shandong Province, China (No. tshw20130955), USDA NIFA McIntire-Stennis Program (MAS 00028), and NSF (CBET 1739884).

■ REFERENCES

(1) Lehmann, J. A handful of carbon. *Nature* **2007**, *447*, 143−144.
(2) Ahmad, M.; Rajapaksha, A. U.; Lim, J. E.; Zhang, M.; Bolan, N.; Mohan, D.; Vithanage, M.; Lee, S. S.; Ok, Y. S. Biochar as a sorbent for contaminant management in soil and water: a review. *Chemosphere* **2014**, *99*, 19−33.
(3) Lian, F.; Xing, B. Black carbon (biochar) in water/soil environments: molecular structure, sorption, stability, and potential Risk. *Environ. Sci. Technol.* **2017**, *51*, 13517−13532.
(4) Gao, X.; Wu, H. Aerodynamic properties of biochar particles: Effect of grinding and implications. *Environ. Sci. Technol. Lett.* **2014**, *1*, 60−64.
(5) Spokas, K. A.; Novak, J. M.; Masiello, C. A.; Johnson, M. G.; Colosky, E. C.; Ippolito, J. A.; Trigo, C. Physical disintegration of biochar: An overlooked process. *Environ. Sci. Technol. Lett.* **2014**, *1*, 326−332.
(6) Wang, D.; Zhang, W.; Hao, X.; Zhou, D. Transport of biochar particles in saturated granular media: effects of pyrolysis temperature and particle size. *Environ. Sci. Technol.* **2013**, *47*, 821−828.
(7) Chen, M.; Wang, D.; Yang, F.; Xu, X.; Xu, N.; Cao, X. Transport and retention of biochar nanoparticles in a paddy soil under environmentally-relevant solution chemistry conditions. *Environ. Pollut.* **2017**, *230*, 540−549.
(8) Chen, M.; Alim, N.; Zhang, Y.; Xu, N.; Cao, X. Contrasting effects of biochar nanoparticles on the retention and transport of

DOI: 10.1021/acs.est.8b01481
Environ. Sci. Technol. 2018, 52, 10369−10379

phosphorus in acidic and alkaline soils. *Environ. Pollut.* **2018**, *239*, 562−570.
(9) Kim, H. B.; Kim, S. H.; Jeon, E. K.; Kim, D. H.; Tsang, D. C. W.; Alessi, D. S.; Kwon, E. E.; Baek, K. Effect of dissolved organic carbon from sludge, rice straw and spent coffee ground biochar on the mobility of arsenic in soil. *Sci. Total Environ.* **2018**, *636*, 1241−1248.
(10) Begum, P.; Ikhtiari, R.; Fugetsu, B. Potential impact of multi-walled carbon nanotubes exposure to the seedling stage of selected plant species. *Nanomaterials* **2014**, *4*, 203−221.
(11) Van Der Ploeg, M. J.; Handy, R. D.; Heckmann, L. H.; Van Der Hout, A.; Van Den Brink, N. W. C60 exposure induced tissue damage and gene expression alterations in the earthworm Lumbricus rubellus. *Nanotoxicology* **2013**, *7*, 432−440.
(12) Combarros, R. G.; Collado, S.; Diaz, M. Toxicity of graphene oxide on growth and metabolism of Pseudomonas putida. *J. Hazard. Mater.* **2016**, *310*, 246−252.
(13) Wang, Z.; Xu, L.; Zhao, J.; Wang, X.; White, J. C.; Xing, B. CuO nanoparticle interaction with arabidopsis thaliana: toxicity, parent-progeny transfer, and gene expression. *Environ. Sci. Technol.* **2016**, *50*, 6008−6016.
(14) Zhao, L.; Cao, X.; Mašek, O.; Zimmerman, A. Heterogeneity of biochar properties as a function of feedstock sources and production temperatures. *J. Hazard. Mater.* **2013**, *256−257*, 1−9.
(15) Qu, X.; Fu, H.; Mao, J.; Ran, Y.; Zhang, D.; Zhu, D. Chemical and structural properties of dissolved black carbon released from biochars. *Carbon* **2016**, *96*, 759−767.
(16) Braadbaart, F.; Poole, I.; van Brussel, A. A. Preservation potential of charcoal in alkaline environments: an experimental approach and implications for the archaeological record. *J. Archaeol. Sci.* **2009**, *36*, 1672−1679.
(17) Keiluweit, M.; Nico, P. S.; Johnson, M. G.; Kleber, M. Dynamic molecular structure of plant biomass-derived black carbon (biochar). *Environ. Sci. Technol.* **2010**, *44*, 1247−1253.
(18) Spokas, K. A. Review of the stability of biochar in soils: Predictability of O:C molar ratios. *Carbon Manage.* **2010**, *1*, 289−303.
(19) Yi, P.; Pignatello, J. J.; Uchimiya, M.; White, J. C. Heteroaggregation of cerium oxide nanoparticles and nanoparticles of pyrolyzed biomass. *Environ. Sci. Technol.* **2015**, *49*, 13294−13303.
(20) Wang, H.; Dong, Y. N.; Zhu, M.; Li, X.; Keller, A. A.; Wang, T.; Li, F. Heteroaggregation of engineered nanoparticles and kaolin clays in aqueous environments. *Water Res.* **2015**, *80*, 130−138.
(21) Upendar, S.; Mani, E.; Basavaraj, M. G. Aggregation and stabilization of colloidal spheroids by oppositely charged spherical nanoparticles. *Langmuir* **2018**, *34*, 6511−6521.
(22) Sotirelis, N. P.; Chrysikopoulos, C. V. Heteroaggregation of graphene oxide nanoparticles and kaolinite colloids. *Sci. Total Environ.* **2017**, *579*, 736−744.
(23) Zhao, J.; Liu, F.; Wang, Z.; Cao, X.; Xing, B. Heteroaggregation of graphene oxide with minerals in aqueous phase. *Environ. Sci. Technol.* **2015**, *49*, 2849−2857.
(24) Feng, Y.; Liu, X.; Huynh, K. A.; McCaffery, J. M.; Mao, L.; Gao, S.; Chen, K. L. Heteroaggregation of graphene oxide with nanometer- and micrometer-sized hematite colloids: Influence on nanohybrid aggregation and microparticle sedimentation. *Environ. Sci. Technol.* **2017**, *51*, 6821−6828.
(25) Zheng, H.; Wang, Z.; Zhao, J.; Herbert, S.; Xing, B. Sorption of antibiotic sulfamethoxazole varies with biochars produced at different temperatures. *Environ. Pollut.* **2013**, *181*, 60−67.
(26) Li, W.; Zhu, X.; He, Y.; Xing, B.; Xu, J.; Brookes, P. C. Enhancement of water solubility and mobility of phenanthrene by natural soil nanoparticles. *Environ. Pollut.* **2013**, *176*, 228−233.
(27) Zheng, H.; Wang, Z.; Deng, X.; Zhao, J.; Luo, Y.; Novak, J.; Herbert, S.; Xing, B. Characteristics and nutrient values of biochars produced from giant reed at different temperatures. *Bioresour. Technol.* **2013**, *130*, 463−471.
(28) Li, F.; Cao, X.; Zhao, L.; Wang, J.; Ding, Z. Effects of mineral additives on biochar formation: Carbon retention, stability, and properties. *Environ. Sci. Technol.* **2014**, *48*, 11211−11217.
(29) Li, W.; He, Y.; Wu, J.; Xu, J. Extraction and characterization of natural soil nanoparticles from Chinese soils. *Eur. J. Soil Sci.* **2012**, *63*, 754−761.
(30) Chowdhury, I.; Duch, M. C.; Mansukhani, N. D.; Hersam, M. C.; Bouchard, D. Colloidal properties and stability of graphene oxide nanomaterials in the aquatic environment. *Environ. Sci. Technol.* **2013**, *47*, 6288−6296.
(31) Li, M.; Huang, C. P. Stability of oxidized single-walled carbon nanotubes in the presence of simple electrolytes and humic acid. *Carbon* **2010**, *48*, 4527−4534.
(32) Angın, D. Effect of pyrolysis temperature and heating rate on biochar obtained from pyrolysis of safflower seed press cake. *Bioresour. Technol.* **2013**, *128*, 593−597.
(33) Manikandan, A.; Subramanian, K. S.; Pandian, K. Effect of high energy ball milling on particle size and surface area of adsorbents for efficient loading of fertilizer. *Asian J. Soil Sci.* **2013**, *8*, 249−254.
(34) Major, J. Guidelines on practical aspects of biochar application to field soil in various soil management systems. *International Biochar Initiative* **2010**, 8.
(35) Bougrier, C.; Carrère, H.; Delgenès, J. P. Solubilisation of waste-activated sludge by ultrasonic treatment. *Chem. Eng. J.* **2005**, *106*, 163−169.
(36) Mohanty, S. K.; Boehm, A. B. Effect of weathering on mobilization of biochar particles and bacterial removal in a stormwater biofilter. *Water Res.* **2015**, *85*, 208−215.
(37) Luo, Y.; Durenkamp, M.; De Nobili, M.; Lin, Q.; Brookes, P. C. Short term soil priming effects and the mineralisation of biochar following its incorporation to soils of different pH. *Soil Biol. Biochem.* **2011**, *43*, 2304−2314.
(38) Lehmann, J.; Kuzyakov, Y.; Pan, G.; Ok, Y. S. Biochars and the plant-soil interface. *Plant Soil* **2015**, *395*, 1−5.
(39) Liu, G.; Chen, L.; Jiang, Z.; Zheng, H.; Dai, Y.; Luo, X.; Wang, Z. Aging impacts of low molecular weight organic acids (LMWOAs) on furfural production residue-derived biochars: Porosity, functional properties, and inorganic minerals. *Sci. Total Environ.* **2017**, *607−608*, 1428−1436.
(40) Kercher, A. K.; Nagle, D. C. Microstructural evolution during charcoal carbonization by X-ray diffraction analysis. *Carbon* **2003**, *41*, 15−27.
(41) Han, J.; Kwon, J. H.; Lee, J.-W.; Lee, J. H.; Roh, K. C. An effective approach to preparing partially graphitic activated carbon derived from structurally separated pitch pine biomass. *Carbon* **2017**, *118*, 431−437.
(42) Zhang, M.; Gao, B.; Chen, J.; Li, Y. Effects of graphene on seed germination and seedling growth. *J. Nanopart. Res.* **2015**, *17*, 78.
(43) Stankovich, S.; Dikin, D. A.; Piner, R. D.; Kohlhaas, K. A.; Kleinhammes, A.; Jia, Y.; Wu, Y.; Nguyen, S. T.; Ruoff, R. S. Synthesis of graphene-based nanosheets via chemical reduction of exfoliated graphite oxide. *Carbon* **2007**, *45*, 1558−1565.
(44) Harvey, O. R.; Kuo, L. J.; Zimmerman, A. R.; Louchouarn, P.; Amonette, J. E.; Herbert, B. E. An index-based approach to assessing recalcitrance and soil carbon sequestration potential of engineered black carbons (biochars). *Environ. Sci. Technol.* **2012**, *46*, 1415−1421.
(45) Saleh, N. B.; Pfefferle, L. D.; Elimelech, M. Aggregation kinetics of multiwalled carbon nanotubes in aquatic systems: measurements and environmental implications. *Environ. Sci. Technol.* **2008**, *42*, 7963−7969.
(46) Chen, K. L.; Elimelech, M. Aggregation and deposition kinetics of fullerene (C60) nanoparticles. *Langmuir* **2006**, *22* (26), 10994−11001.
(47) Chowdhury, I.; Mansukhani, N. D.; Guiney, L. M.; Hersam, M. C.; Bouchard, D. Aggregation and stability of reduced graphene oxide: Complex roles of divalent cations, pH, and natural organic matter. *Environ. Sci. Technol.* **2015**, *49*, 10886−10893.
(48) Konkena, B.; Vasudevan, S. Understanding aqueous dispersibility of graphene oxide and reduced graphene oxide through pKa measurements. *J. Phys. Chem. Lett.* **2012**, *3*, 867−872.
(49) Smith, B. M.; Pike, D. J.; Kelly, M. O.; Nason, J. A. Quantification of heteroaggregation between citrate-stabilized gold

DOI: 10.1021/acs.est.8b01481
Environ. Sci. Technol. 2018, 52, 10369−10379

nanoparticles and hematite colloids. *Environ. Sci. Technol.* **2015**, *49*, 12789−12797.
(50) Liu, G.; Zheng, H.; Jiang, Z.; Wang, Z. Effects of biochar input on the properties of soil nanoparticles and dispersion/sedimentation of natural mineral nanoparticles in aqueous phase. *Sci. Total Environ.* **2018**, *634*, 595−605.
(51) Sarpong, L. K.; Bredol, M.; Schönhoff, M. Heteroaggregation of multiwalled carbon nanotubes and zinc sulfide nanoparticles. *Carbon* **2017**, *125*, 480−491.
(52) Lin, Y.; Munroe, P.; Joseph, S.; Kimber, S.; Van Zwieten, L. Nanoscale organo-mineral reactions of biochars in ferrosol: An investigation using microscopy. *Plant Soil* **2012**, *357*, 369−380.
(53) Warnock, D. D.; Lehmann, J.; Kuyper, T. W.; Rillig, M. C. Mycorrhizal responses to biochar in soil − concepts and mechanisms. *Plant Soil* **2007**, *300*, 9−20.
(54) Mukherjee, A.; Zimmerman, A. R.; Hamdan, R.; Cooper, W. T. Physicochemical changes in pyrogenic organic matter (biochar) after 15 months field-aging. *Solid Earth* **2014**, *6*, 731−760.
(55) Masiello, C. A.; Chadwick, O. A.; Southon, J.; Torn, M. S.; Harden, J. W. Weathering controls on mechanisms of carbon storage in grassland soils. *Global Biogeochem. Cy.* **2004**, *18*, GB4023.
(56) Freixa, A.; Acuna, V.; Sanchis, J.; Farre, M.; Barcelo, D.; Sabater, S. Ecotoxicological effects of carbon based nanomaterials in aquatic organisms. *Sci. Total Environ.* **2018**, *619−620*, 328−337.
(57) Ema, M.; Hougaard, K. S.; Kishimoto, A.; Honda, K. Reproductive and developmental toxicity of carbon-based nanomaterials: A literature review. *Nanotoxicology* **2016**, *10*, 391−412.

DOI: 10.1021/acs.est.8b01481
Environ. Sci. Technol. 2018, 52, 10369−10379